Hindawi
International Journal of Antennas and Propagation
Volume 2019, Article ID 9454271, 10 pages
https://doi.org/10.1155/2019/9454271

Research Article

Large-Scale Channel Modeling and Measurements for 10 GHz in Indoor Environments

Iury S. Batalha, Andréia V. R. Lopes, Jasmine P. L. Araújo, Fabrício J. B. Barros, Bruno L. S. Castro, Gervásio P. S. Cavalcante, and Evaldo G. Pelaes

LCT, UFPA, Belem 66045-110, Brazil

Correspondence should be addressed to Iury S. Batalha; iurybatalha@gmail.com

Received 31 August 2018; Accepted 11 November 2018; Published 23 January 2019

Guest Editor: Peter Excell

With the advent of 5G mobile communication and researches into the propagation of large-scale channel modeling for frequencies above 6 GHz, measurement investigation was performed at 10 GHz with horn-type directional antennas in a corridor and a computer room within the Electrical and Computer Engineering Laboratories' first floor, at Federal University of Pará (UFPA), Brazil. This paper presents data obtained through experimental work, channel modeling with co-polarization V-V and H-H and cross-polarization V-H in line-of-sight (LOS) or non-line-of-sight (NLOS) conditions. The large-scale close-in reference is sustained by a comprehensive analysis, considering propagation mechanisms such as reflection and diffraction. Results demonstrate that the established model had inferior standard deviation in relation to measured data, proving itself more significant to propagation in indoor environments.

1. Introduction

The considerable quantity of bandwidth available in frequency bands above 6 GHz is an attractive resource to provide multi-Gigabit per second (Gbps) data rates. Such resource would alleviate the traffic flow of mobile data in lower frequency bands, such as those below 6 GHz [1, 2]. With the advent of the new generation of mobile communication (5G), there is a great deal of research taking place into the development to provide recommendations. One of its branches of study lies within the millimetric waves, resulting in works above 6 GHz [3–6]. Frequencies within 3 to 30 GHz (SHF: Super High Frequency) and 30 to 300 (EHF: Extremely High Frequency) bands present similar propagation characteristics, classifying them as millimetric wave (mmWave) bands [4, 5]. Therefore, it is fundamental to know the mmWave channel's propagation characteristics for the development of fifth generation mobile and wireless communication systems—5G [7].

These channel propagation characteristics can be defined through path loss models, in large scale, that predict the propagation signal's attenuation according to distance. They are important for developing more efficient communication systems, to optimize the positioning of transmitting antennas and assist on future telecommunication system projects [8].

For indoor environments, there are several structural questions that influence signal behavior, such as construction materials utilized in the building, size of building/rooms/corridors, number of people circulating inside the room, furniture types and placement, and interference with other systems. They confine the waves within the environment, leading to more reflective components and multiple paths for the signal to propagate, as well as crossing of walls (diffraction) and other types of obstacles [9].

A wireless system requires extensive research and comprehension of its propagation channels. Even though a large number of investigations have been undertaken into channels below 6 GHz, there are campaigns aiming at measuring and modeling of 5G channels at 10 to 28 GHz and 30 to 72 GHz bands [5, 10–15], presented by institutes such as New York University (NYU) and the Mobile and Wireless Community Enablers for the Twenty-Twenty Information Society (METIS)—the former created with the sole purpose to standardize 5G systems [16, 17]. The METIS report

identifies probable bands for 5G application; 10 GHz is listed as a promising frequency band.

As an example of a study based in measuring frequencies above 6 GHz, Deng et al. developed models for diffraction and signal strength measurements around sharp-edged objects such as corners, pillars, and irregular surfaces, for the 10, 20, and 26 GHz spectrum. The diffraction measurements were made in closed and exterior environments, using a continuous wave (CW) probe with three pairs of identical horn-type directional antennas at the transmitter and receptor [18].

In 2014, Kim et al. studied large-scale parameters based on various indoor environments at 11 GHz, comprising path-loss polarization characteristics, shadowing, cross-polarization power ratio, delay spread, and coherence bandwidth [19].

Reference [20] presents radio channel characteristics on carrier frequencies 11.2 and 14.6 GHz, with a 1 GHz bandwidth in environments simulated as a corridor, a laboratory, offices, and a conference room inside a building in Beijing, China. There, investigations regarding large- and small-scale fading properties were conducted, based on realistic measurements. Propagation and delay correlations were also discussed.

Ling et al. produced a measurement campaign of channels implementing directional sweeping to capture temporal and spatial propagation characteristics for upper frequencies, from 13 to 17 GHz, in classroom environments [21].

In [13], there are large-scale models and measuring of frequencies 14 and 22 GHz within line-of-sight (LOS) and non-line-of-sight (NLOS) conditions. A dual-slope model is suggested to distinguish the channel—its validity is proven through the close-in free space reference model, and its parameters defined by MMSE (Minimum Mean Square Error). Another approach is a model inspired in waveguide measurements.

Properties of a channel at the 20 GHz band for an office environment are shown in [22]. Measurements were made using a channel probe at the 20 GHz spectrum, with an orthogonal frequency division multiplexing signal and a bandwidth of 50 MHz. Characteristics of omnidirectional antennas were obtained by turning directional antennas through the azimuthal axis and elevated to the receptor's side.

Reference [23] exposes several large-scale measurements utilizing high-gain directional antennas at 28 and 73 GHz. A model that simulates an omnidirectional antenna in which high-gain antennas were rotated a whole 360 degrees in both Tx and Rx is also described in this paper. This took place in offices with line-of-sight (LOS) and non-line-of-sight (NLOS), with copolarization (V-V) and cross-polarization (V-H). For large-scale models, templates were utilized, such as CI, CIX, CIF, CIFX, FI, ABG, and ABGX, in which the path loss exponent (n) is defined through MMSE (Minimum Mean Square Error). The model's random variable has an average value of zero, and standard deviation of measured data is given in decibels. Results show that the models have great accuracy when compared to measured data.

Lei et al. have proposed a measurement system at 28 GHz in 3 different scenarios, including an office, a corridor, and a generic hall, using 26 dBi directional antennas and a VNA to analyze the channel at a maximum distance of 30 meters. The three properties which were analyzed are path loss, RMS delay spread, and the power angular profiles (PAPs). Results illustrate that indoor environments can enhance the received signal power in the case of LOS. However, in case of NLOS, the penetration loss caused by walls and doors can bring considerable attenuation, which implies that minor cells will have an important role increasing the probability of LOS links for future communication systems. Multipath components (MPCs) can be detected from many directions, albeit needing to use high-directivity antennas [24].

MacCartney et al. compiled a comprehensive study on path loss models of simple or multifrequency mmWave, based on layouts for polarization of separate antennas, and combined in LOS and NLOS environments for three common office layouts. The frequency channels used are 28 GHz and 73 GHz [23].

In [25], Geng et al. made propagation measurements at 60 GHz in several indoor environments, with continuous route (CR) and direction-of-arrival (DOA) measurement campaigns. The propagation mechanisms were studied based on DOA data, indicating that direct waves and the first-order reflected waves on smooth surfaces were sufficient in a LOS environment. Whereas in NLOS cases, diffraction was highly significant, and the propagation loss through walls was very high.

The objective of our study is to present a statistical large-scale analysis of measured data in indoor environments at the 10 GHz spectrum. Signal behavior for LOS and NLOS is specified in two different rooms, with antenna copolarization (V-V and H-H) and cross-polarization (V-H).

The paper is organized as follows. Section 2 presents all measurement equipment utilized during the campaigns, the mounted scenarios, and all measurement procedures; Section 3 elucidates the modeling analysis, the proposed large-scale model for path loss and the obtained results in comparison to other models found in the literature; Section 4 provides discussions and conclusions on the obtained data.

2. Measurement Investigations

This section describes the transmitting and receiving equipment, the scenarios considered for the measurement campaigns, and line-of-sight (LOS)/non-line-of-sight (NLOS) measurements. It also contains information about copolarization (V-V) and (H-H) and cross-polarization for both studied environments.

2.1. Equipment and Setup. Two identical horn-type directional antennas were utilized, fabricated by MCS Industries, with gain of 15 dBi, apertures of 29 degrees on the horizontal plain and 29.3 degrees on the vertical plain, and 1.7 meters above the floor. For the transmitting equipment (Tx), a continuous wave (CW) signal generator (Hewlett Packard© Synthesized Sweeper 83752A) was chosen, sweeping frequencies from 1 to 20 GHz. The Tx was fixed, the environment, remaining immobile, and configured with transmission

powers of 0 dBm for V-V and H–H and 15 dBm for V-H. The selected receptor (Rx), however, was an Anritsu© Signal Analyzer MS2692A.

For the first iteration, Tx and Rx were positioned with a distance of 1 meter from each other. And for the subsequent iterations, the distance between Tx and Rx is increased by another 1 meter. It is important to note that these experiments occurred with no objects or persons obstructing the transmitted beam. Table 1 provides specifications of equipment and parameter configurations for the campaigns.

2.2. Corridor. The corridor, depicted in Figure 1, has dimensions of 15.22 m × 1.37 m. It is built out of brick walls and smooth concrete on the floor, also containing wooden doors, metallic grilles, and containers with power supplies and circuit breakers. The transmitter Tx was fixed at a distance of 1.3 meters from the windowed wall, whereas Rx was progressively moved 1 meter away from Tx for every iteration of the experiment.

For the corridor, approximately 10 power values were measured for each of the 14 measuring points. For each one, 10,001 power data were collected for each meter variation. The procedure was repeated 10 times for each point, resulting in 100.010 power data for each iteration (10 × 10,001). Therefore, 1,400,140 power data were collected at the corridor environment (100,010 × 14 points).

The quantity of measured points by polarization type is distinct for each one. For vertical polarization (V-V) all 14 points were measured. For horizontal polarization (H-H) only 10 measured points were used, and with cross-polarization (V-H) only 8 points were measured. The amount of measured points for H-H and V-V was recorded for each distance until the signal strength reached noise level.

2.3. Computer Room. The computer room's dimensions are 14.97 m × 7.67 m. As configured in the corridor, Tx was placed in a fixed position 1.3 meters away from the wall, also moving Rx away from Tx by 1 meter every iteration. This room is constituted of brick/concrete walls and drywalls, containing glass windows, wood tables, metallic chairs, and evenly disposed desktops, as shown in Figure 2.

The laboratory was chosen because it presents different characteristics comparing with the corridor; the corridor presents a length much larger than the wavelength of the frequencies used, providing greater reflection in this environment; on the other hand the lab presents a smaller length and walls with different compositions; it is formed for masonry walls and wood, for the walls of masonry the reflections are close to that seen in the corridor, and the wooden ones there have less reflection compared to the masonry wall. Therefore, the laboratory is an interesting environment to determine the loss behavior because it is formed by different types of materials and that directly influence the behavior of the signal received in the Rx.

In this environment, a radial component was defined at 3.8 meters away from the lateral walls. In each radial, 10 power values for each of the 12 traced points were measured. Given that 100,010 power data are obtained in every iteration, as previously noted, the total amount of power data extracted reaches 1,200,120. In contrast to the corridor, all 12 points distributed along the room were measured for all polarization configurations (V-V, H-H, and V-H).

For the measurement campaign utilizing copolarized antennas (V-V and H-H), horn-type directional antennas were also used, with 15 dBi gain on both Tx/Rx and a transmission power of 0 dBm. For cross-polarization, the gain is also 15 dBi on Tx/Rx; however, the transmission power is 15 dBm.

3. Large-Scale Path Loss Models

Large-scale path loss models predict loss according to the distance between the transmitter and the receptor. These models are important for wireless telecommunication projects [8], aiding the analysis of wave propagation through indoor environments, as there are multiple wave deviation events like multipath, reflection, diffraction, penetration, and shadowing—that is, attenuators of received power at Rx [26]. They also provide realistic propagation characteristics for a wireless channel [5, 10–28]. Most models assume loss in a logarithmic scale. Parameters for the models utilized in this study were defined through MMSE, and the close-in free space model (with its extensions) was utilized for approximation.

The close-in (CI) free space path loss model as seen in (1) and given in dB is uniquely parametrized by a sole variable known as the path loss exponent (PLE), or n. This CI model has a physical distance reference represented by d_0. The loss model parameters are determined by MMSE, minimizing error between measured and simulated data. In this work, the distance reference is set to 1 meter, and the model can be applied to estimate path loss in both cross- and copolarization conditions.

$$\mathrm{PL}^{\mathrm{CI}}(f,d)[\mathrm{dB}] = \mathrm{FSPL}(f,d_0) + 10n_{\mathrm{V\text{-}V}}\log_{10}\left(\frac{d}{d_0}\right) + X_\sigma^{\mathrm{CI}}, \tag{1}$$

$$\mathrm{FSPL}(f,d_0) = 10\log_{10}\left(\frac{4\pi d_0}{\lambda}\right)^2, \tag{2}$$

where X_σ^{CI} is a random variable of the Gaussian type with an average value of zero and standard deviation in dB, $n_{\mathrm{V\text{-}V}}$ is the path loss exponent for copolarization and FSPL is the initial loss found in the model defined by (2). λ is the wavelength and d_0 is the previously explained reference distance, set to 1 m.

The CI model possesses an extension for the case of cross-polarization (3), adding a factor called cross-polarization discrimination (XPD). This parameter is defined via MMSE [28–30]. The equation then becomes

$$\mathrm{PL}^{\mathrm{CIX}}(f,d)[\mathrm{dB}] = \mathrm{FSPL}(f,d_0) + 10n_{\mathrm{V\text{-}H}}\log_{10}\left(\frac{d}{d_0}\right) + X_\sigma^{\mathrm{CIX}} + \mathrm{XPD}[\mathrm{dB}], \tag{3}$$

Table 1: Channel sounding system specifications for the 10 GHz indoor measurement campaign.

Parameters	Configurations	Units
Central frequency	10	GHz
Signal transmission	Continuous wave	—
Antennas	Horn-type, directional	—
Transmitted copolarization power	0	dBm
Transmitted cross-polarization power	15	dBm
Antenna height for Tx/Rx	1.7	m
Antenna gain for Tx/Rx	15	dBi
Azimuthal HPBW for Tx/RX	29	Degrees
HPBW elevation for Tx/Rx	29.3	Degrees

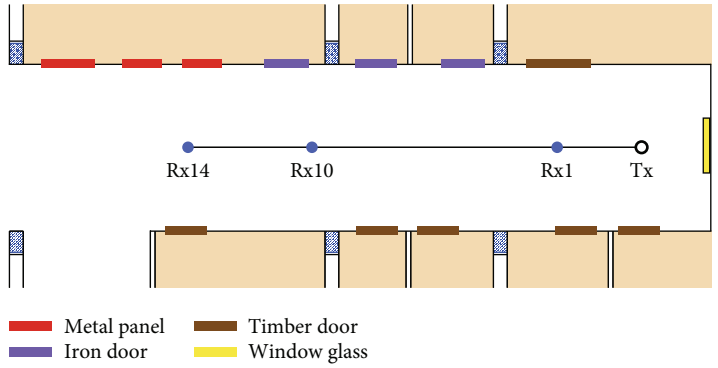

Figure 1: Distance for Tx as done.

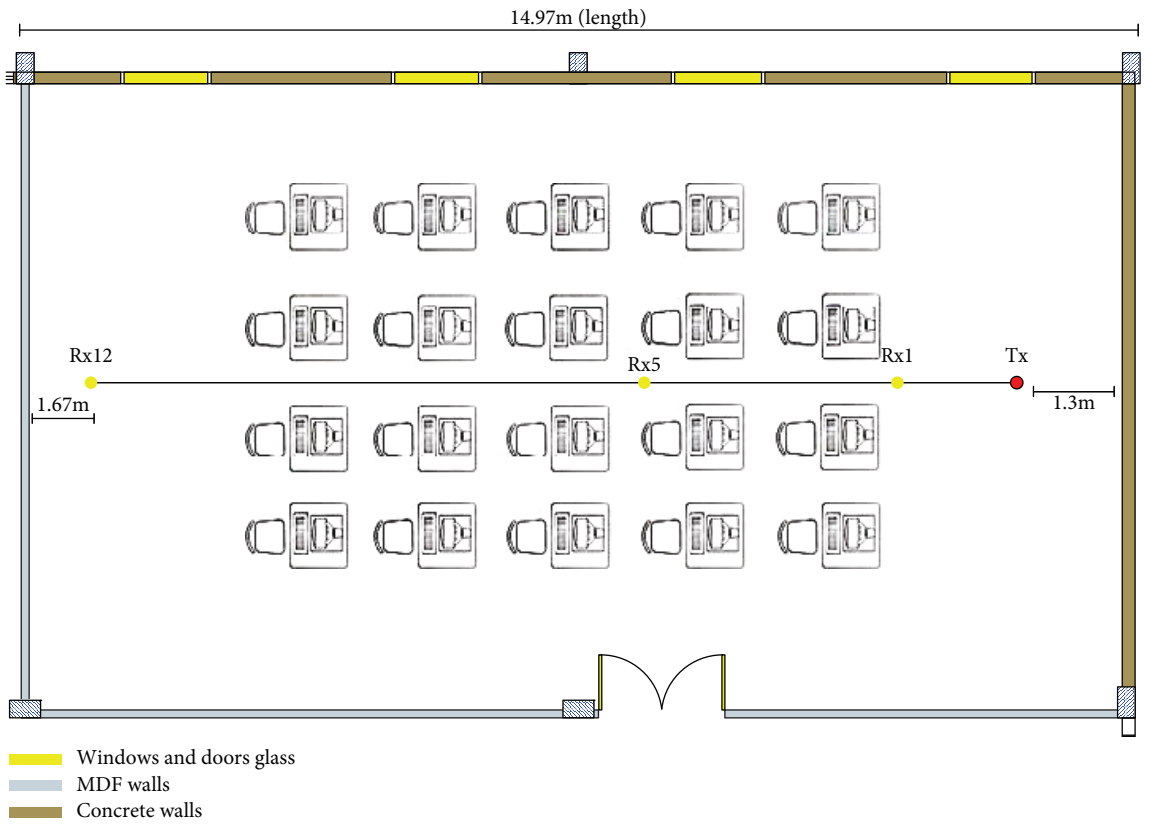

Figure 2: The computer room's blueprint.

in which XPD is represented in dB, and $X_{\sigma}^{\mathrm{CIX}}$ is a Gaussian random variable with average value of zero and standard deviation in dB. n used in this calculation has to be defined in the measured data in the cross-polarization configuration. Maccartney et al. [23] utilize $n_{\mathrm{V\text{-}V}}$ for the model that considers cross-polarized antennas (CIX), in this paper, $n_{(\mathrm{V\text{-}H})}$ is used to adjust to a slope of the curve.

Another independent extension for the CI model is the case of copolarized H-H configuration, adding a path loss parameter for H-H copolarization (4). This parameter is similar to XPD and also defined through MMSE.

$$\mathrm{PL}^{\mathrm{CIHH}}(f,d)[\mathrm{dB}] = \mathrm{FSPL}(f,d_0) + 10n_{\mathrm{H\text{-}H}}\log_{10}\left(\frac{d}{d_0}\right) + X_{\sigma}^{\mathrm{CI}}. \tag{4}$$

In (4), $n_{\mathrm{H\text{-}H}}$ represents the copolarized H-H path loss exponent (PLE), and $X_{\sigma}^{\mathrm{CIHH}}$ is a Gaussian random variable with average value of zero and standard deviation in dB.

The last proposed extension illustrated for the CI model is the obstacle path loss exponent (OPLE), in which an attenuation parameter signifying obstruction by same or distinct obstacles found in the propagation's path.

$$\mathrm{PL}^{\mathrm{CI}}(f,d)[\mathrm{dB}] = \mathrm{FSPL}(f,d_0) + 10n_{v\_v}\log_{10}\left(\frac{d}{d_0}\right) + X_{\sigma}^{\mathrm{CI}} + \sum_{i=1}^{i}\mathrm{OPLE}_i(np_i), \tag{5}$$

in which OPLE_i is the obstacle path loss exponent, and i corresponds to the quantity of same-type obstacles. This parameter is based on the COST-231 Motley-Keenan model.

4. Modeling and Result Analysis

In this section, there is an analysis of signal attenuation behavior in relation to the measured path loss for both studied scenarios. The complexity of indoor environments generates multiple paths—reflections, diffractions, penetration effects, and shadowing—that have significant impact on received power [31]. Radio signal attenuation in waveguides (or for instance, tunnels and corridors) is generally much lower than in free space and is inversely proportional to frequency due to the wave orientation effect.

About the measured data, PLE, standard deviation, and XPD values were defined through MMSE. Table 2 presents the said values. Table 3 presents values for OPLE for different types of walls.

4.1. Corridor Analysis. Figure 3 presents data modeled through the CI model for V-V and H-H polarizations and CIX for V-H, in which the PLE is the gradient of the straight line that shows how the signal degrades with distance, also directly influencing the standard deviation values of measured data in the corridor. Figure 4 illustrates the shadowing effect defined by the random variable for directional antennas, where it is observed that the model has a good approximation compared to measured data and checking the simulated signal's variability between Tx and Rx. Figure 5 shows point-to-point standard deviation data, verifying signal variation for each travelled meter in the environment for all 3 polarizations.

Table 2: PLE values for each polarization in the corridor and in the laboratory.

Scenario	Polarization	PLE	σ (dB)	XPD (dB)
Laboratory	V-V	1.55	6.56	22.30
	H-H	1.64	6.12	
	V-H	0.08	4.23	
Corridor	V-V	1.96	5.6	21.30
	H-H	1.81	5.48	
	V-H	0.65	2.39	

Table 3: Loss per wall for 10 GHz indoor measurement campaign.

Frequency	Masonry	Wood	Glass
10 GHz	10 (dB)	2 (dB)	0 (dB)

Figure 3 presents measured data for the 3 polarization types (V-V, H-H, and V-H), and for the close-in model with extensions for the 10 GHz band, data in blue and red represent the values for copolarized antennas, in which PLE values are very close to 1.96 dB and 1.81 dB for V-V and H-H configurations, respectively (the major difference between them is the initial loss). In Figure 3 the data depicted in green are the cross-polarized measured results, where initial loss is substantially higher and lower PLE is observed compared to copolarization.

The channel's variability is represented by a Gaussian random variable, influenced by the shadowing effect and defined for the close-in free space reference path loss model (1). Figure 4 shows the shadowing effect defined by the random variable for directional copolarized antennas (V-V) in the corridor at 10 GHz. It is possible to denote that the loss model (1) has a very good approximation in relation to measured data, checking the simulated signal's variation between Tx and Rx.

An important approach to measured data is the statistical survey with standard deviation. For this purpose, a point-to-point standard deviation was calculated to verify signal variation for each travelled meter between Tx and Rx for both environments utilizing copolarized and cross-polarized configurations. Figure 5 illustrates point-to-point standard deviation simultaneously for all polarizations.

For the data in red in Figure 5, it is possible to observe a low variability in standard deviation values (on the y-axis) with values between 0 and 0.7 dB. This indicates that there is low variability of received power values for a same point utilizing horn-type V-V copolarized antennas in the corridor. In black, standard deviation values for H-H copolarization are shown, presenting a variability equivalent to V-V configuration and confirming that signal variation is also low in this case. The same approach has been applied for cross-polarization data in the corridor (blue-colored triangles), however yielding higher signal variability ranging from 0 to 3.5 dB.

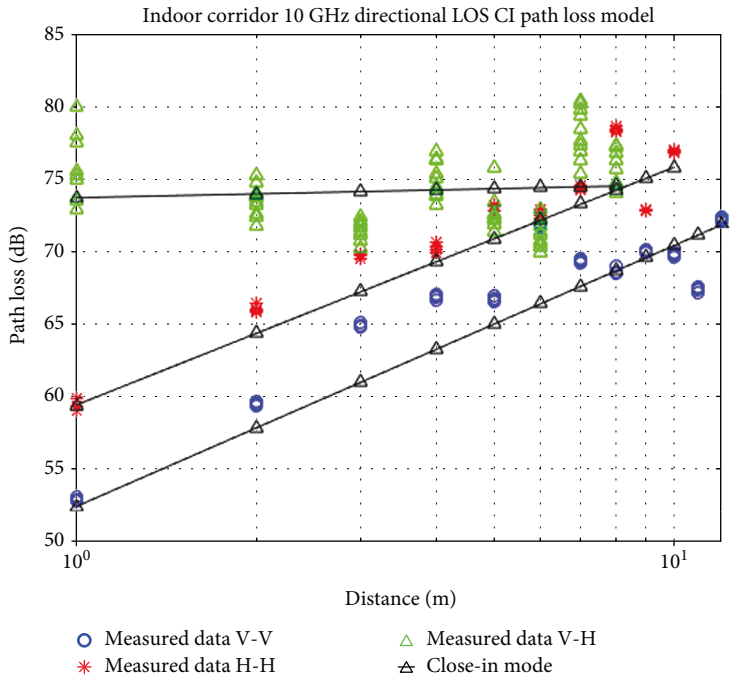

Figure 3: 10 GHz directional LOS large-scale CI path loss model with copolarization V-V, H-H, and V-H in the corridor.

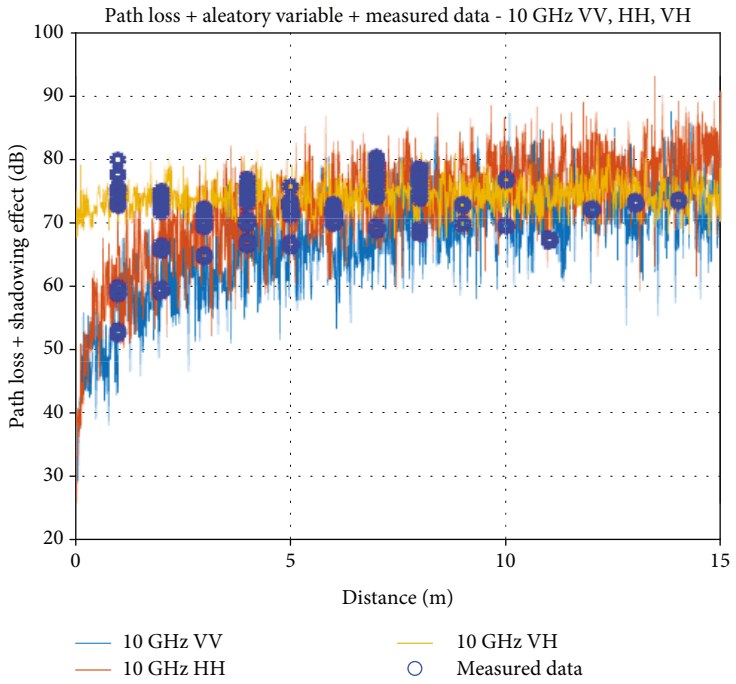

Figure 4: Path loss model CI with shadowing effect at measured data for 10 GHz band in corridor scenario.

It is important to acknowledge that the whole behavior's standard deviation presented higher values for copolarization (V-V and H-H) and lower ones for cross-polarization (V-H). This is directly linked to PLE, in which V-H antennas had PLE values below 1, whilst copolarized V-V and H-H presented values above 1. Consequently, point-to-point standard deviation analysis is important, as it reveals how much the received power varies through measured points.

4.2. Computer Room Analysis. Using the same approach as for the corridor of analysis of the corridor, the computer room measurements have modeled data with CI and CIX

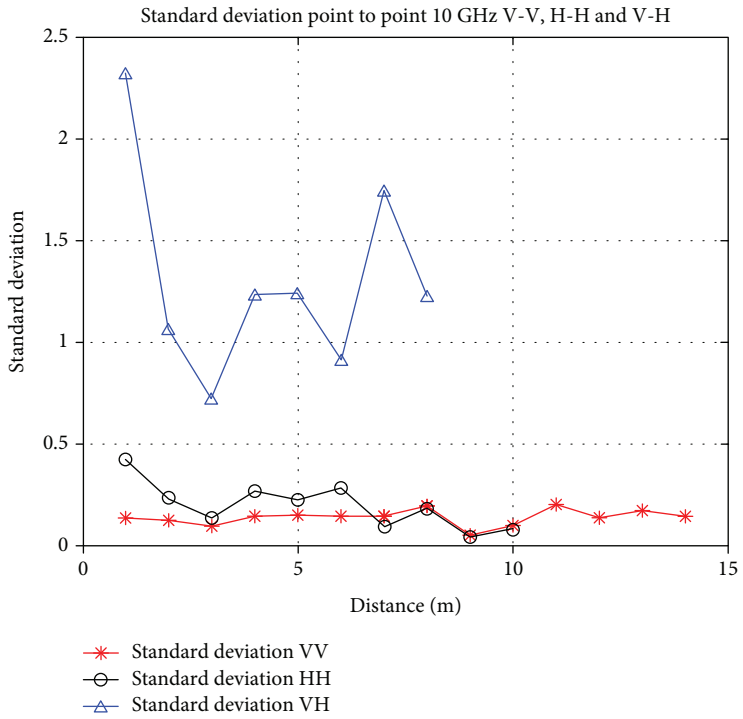

Figure 5: Standard deviation point-to-point data measured in the corridor to V-V, H-H, and V-H.

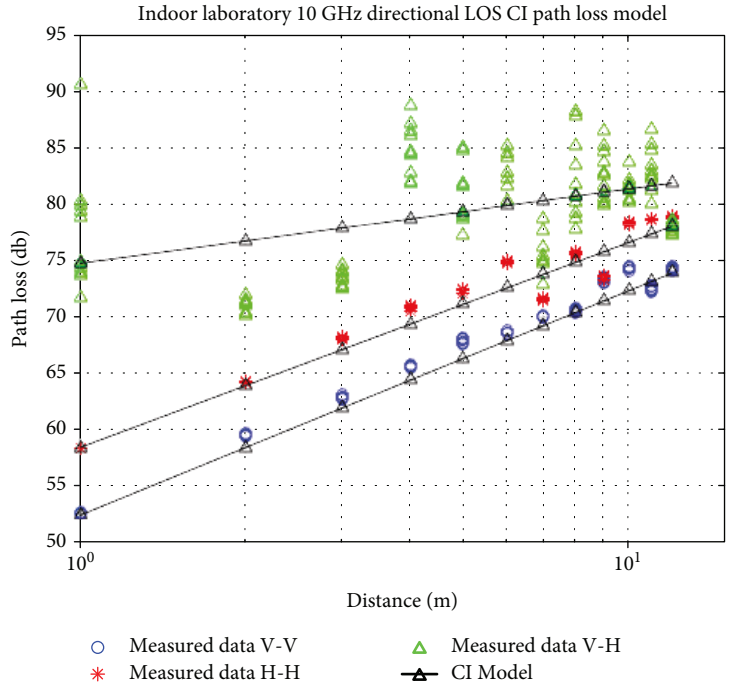

Figure 6: 10 GHz directional LOS large-scale CI path loss model with copolarization V-V, H-H, and V-H in the computer room.

models in logarithmic scale with all polarizations. The PLE also represents the slope's inclination and demonstrates how the signal attenuates with distance and directly influences standard deviation values measured in the computer room.

Figure 6 depicts measured data for all three polarizations and the close-in model with its extensions for 10 GHz propagation. Data in blue and red present data for copolarized antennas in which PLE values are close to 1.55 dB and 1.64 dB for V-V and H-H, respectively. In

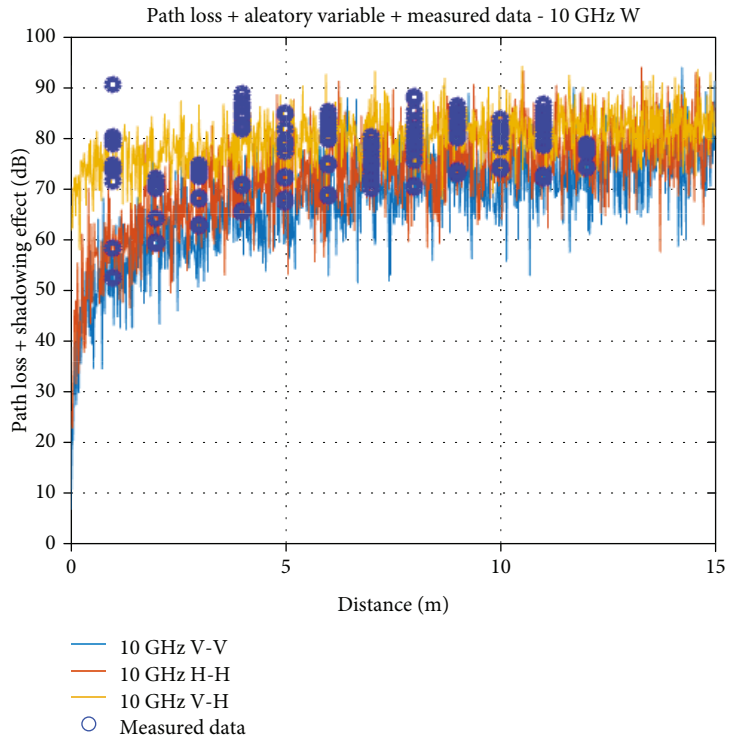

Figure 7: Path loss model CI with shadowing effect at measured data for 10 GHz band in laboratory scenario.

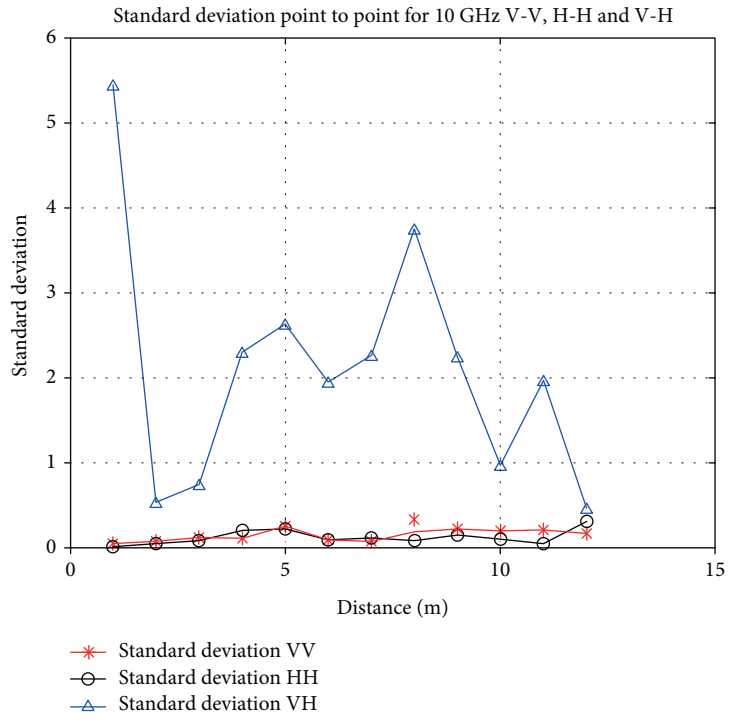

Figure 8: Standard deviation for point-to-point data measured in the computer room to polarizations V-V, H-H, and V-H.

Figure 6 again, the difference is mostly noted on initial losses, for the cross-polarized antenna data set, shown in green, PLE values are lower and the initial losses higher in relation to the copolarized counterparts.

The shadowing effect defined by the random variable for directional antennas and signal variability between Tx and Rx is presented in Figure 7; Figure 8 shows point-to-point measured standard deviation data for signal variation

checking in each meter travelled in the environment for all three polarizations, respectively.

The analysis of the data measured by the standard deviation point-to-point is made with the objective of verifying the variation of the signal for each point measured in all the polarizations. Figure 8 depicts standard variation simultaneously for V-V, H-H, and V-H configurations. The red set of data presents the point-to-point approach at 10 GHz with V-V polarization, and the minimum/maximum observed values in the Y axis range from 0.04 to 0.26 dB. This indicates that there is low variability on received power values for the same point whilst using horn-type V-V copolarized antennas in the computer room. For the black points in the graph, it is the standard deviation for H-H configuration, presenting variability equivalent to V-V, elucidating that measured data vary very little on a point-to-point basis with minimum/maximum values of approximately 0.04–1.05 dB. For the cross-polarization data in the computer room (in green), the standard deviation varies from 0.5 and 5.5 dB, which is evidently greater than the values for copolarized antennas.

5. Conclusions

This paper had the objective to demonstrate channel modeling with path loss model close-in and its extensions, to characterize future wireless network channels. The close-in model presents good approximations in LOS and NLOS conditions with directional horn antennas in cross- and copolarization for the corridor and the computer room at 10 GHz, one of METIS-determined frequencies. PLE values in both environments utilizing directional V-V antennas are close to the ones seen in the literature [14, 27]; however, the values for cross-polarized (V-H) configurations are less than the copolarized values. Another important remark is the analysis of the standard deviation, both in average value or point-to-point. For the average standard deviation, the values favor copolarization (V-V and H-H) in comparison to cross-polarization (V-H) due to low PLE value, as shown in Table 2. When the analysis is point-to-point, the copolarizations have less variation in relation to cross-polarization.

On the point-to-point standard deviation for the corridor environment, it was verified that copolarized antennas V-V and H-H provide low variation, between 0.04 and 1.05 dB, as depicted in Figure 5. For cross-polarization there is more variability, in values ranging from 0 to 3.5 dB, also shown in Figure 5. For the measurements made in the computer room, it is valid to pinpoint that the H-H polarization's standard deviation yields more variability than its V-V counterpart. In a point-to-point analysis, the V-V configuration varies between 0.04 and 0.26 dB, and H-H gives a standard deviation ranging from 0.04 to 1.05 dB, as evident in Figure 8.

The walls also had different influences in each obstacle—its attenuation changes according to the used frequency, being directly proportional to the suffered loss. This is an important point, and future access technologies must work around this problem, given that the new generations of telecommunication systems are bound to evolve to mmWave bands.

Another significant point is the difference in wave propagation within distinct indoor environments. Inside the corridor, wave reflections are heightened due to the proximity of the walls, the material used inside the walls, floor, and ceiling, in addition to grilles and metallic panels. The computer room is a larger environment, with a different composition. It contains drywall and masonry walls as well as chairs, tables, and desktops. These characteristics affect the path loss of electromagnetic waves inside these environments, as this paper displayed its distinctions through the close-in free space loss models and its extensions beyond the standard deviation.

Future works will be carried out in this area, such as large-scale modeling for adjacent frequencies to 10 GHz, such as 8 GHz, 9 GHz, 11 GHz, and 12 GHz, for the same environments cited in this work using different measurement, with the transmitter (Tx) with different heights, with 360° Rx rotation to collect multipath signals using co- and cross-polarization antennas. Moreover, we will carry out small-scale modeling for the 8 to 12 GHz frequency band. Finally, a large-scale and small-scale modeling will be executed for millimeter wave bands in the 28 GHz to 93 GHz band indoors.

Data Availability

The data used to support the findings of this study are included within the article.

Conflicts of Interest

The authors declare that there is no conflict of interest regarding the publication of this paper.

Acknowledgments

We would like to thank the Electrical Engineering Post-Graduation Program (PPGEE) at Federal University of Pará (UFPA) for giving the opportunity and materials to produce this study, the National Council for Scientific and Technological Development (CNPq) for the financing, and the National Institute of Science and Technology (INCT) for its support on the research.

References

[1] A. Ghosh, T. A. Thomas, M. C. Cudak et al., "Millimeter-wave enhanced local area systems: a high-data-rate approach for future wireless networks," *IEEE Journal on Selected Areas in Communications*, vol. 32, no. 6, pp. 1152–1163, 2014.

[2] G. R. MacCartney and T. S. Rappaport, "Study on 3GPP rural macrocell path loss models for millimeter wave wireless communications," in *2017 IEEE International Conference on Communications (ICC)*, pp. 1–7, Paris, France, July 2017.

[3] T. S. Rappaport, S. Sun, R. Mayzus et al., "Millimeter wave mobile communications for 5G cellular: it will work!," *IEEE Access*, vol. 1, pp. 335–349, 2013.

[4] Z. Pi and F. Khan, "An introduction to millimeter-wave mobile broadband systems," *IEEE Communications Magazine*, vol. 49, no. 6, pp. 101–107, 2011.

[5] T. S. Rappaport, G. R. MacCartney, M. K. Samimi, and S. Sun, "Wideband millimeter-wave propagation measurements and channel models for future wireless communication system design," *IEEE Transactions on Communications*, vol. 63, no. 9, pp. 3029–3056, 2015.

[6] METIS, *Deliverable D1.4, METIS Channel Models*, 2015.

[7] J. G. Andrews, S. Buzzi, W. Choi et al., "What will 5G be?," *IEEE Journal on Selected Areas in Communications*, vol. 32, no. 6, pp. 1065–1082, 2014.

[8] M. F. Iskander and Zhengqing Yun, "Propagation prediction models for wireless communication systems," *IEEE Transactions on Microwave Theory and Techniques*, vol. 50, no. 3, pp. 662–673, 2002.

[9] H. K. Rath, S. Timmadasari, B. Panigrahi, and A. Simha, "Realistic indoor path loss modeling for regular WiFi operations in India," in *Twenty-third National Conference on Communications (NCC)*, pp. 1–6, Chennai, India, 2017.

[10] J. Huang, C. X. Wang, R. Feng, J. Sun, W. Zhang, and Y. Yang, "Multi-frequency mmWave massive MIMO channel measurements and characterization for 5G wireless communication systems," *IEEE Journal on Selected Areas in Communications*, vol. 35, no. 7, pp. 1591–1605, 2017.

[11] K. Saito, J. I. Takada, and M. Kim, "Characteristics evaluation of dense multipath component in 11GHz-band indoor environment," in *2016 10th European Conference on Antennas and Propagation (EuCAP)*, pp. 1–3, Davos, Switzerland, 2016.

[12] C. Ling, X. Yin, H. Wang, and R. S. Thomä, "Experimental characterization and multipath cluster modeling for 13–17 GHz indoor propagation channels," *IEEE Transactions on Antennas and Propagation*, vol. 65, no. 12, pp. 6549–6561, 2017.

[13] N. O. Oyie and T. J. O. Afullo, "Measurements and analysis of large-scale path loss model at 14 and 22 GHz in indoor corridor," *IEEE Access*, vol. 6, pp. 17205–17214, 2018.

[14] Q. Liao, Z. Ying, and C. Gustafson, "Simulations and measurements of 15 and 28 GHz indoor channels with different array configurations," in *2017 International Workshop on Antenna Technology: Small Antennas, Innovative Structures, and Applications (iWAT)*, pp. 256–259, Athens, Greece, 2017.

[15] C. Ling, X. Yin, H. Wang, and X. Zhang, "Comparison of parametric and nonparametric characterization of 15 GHz propagation channels in indoor environments," in *2016 10th European Conference on Antennas and Propagation (EuCAP)*, pp. 1–5, Davos, Switzerland, 2016.

[16] H. Tullberg, P. Popovski, Z. Li et al., "The METIS 5G system concept: meeting the 5G requirements," *IEEE Communications Magazine*, vol. 54, no. 12, pp. 132–139, 2016.

[17] H. Droste, G. Zimmermann, M. Stamatelatos et al., "The METIS 5G architecture: a summary of METIS work on 5G architectures," in *2015 IEEE 81st Vehicular Technology Conference (VTC Spring)*, pp. 1–5, Glasgow, Scotland, 2015.

[18] S. Deng, G. R. MacCartney, and T. S. Rappaport, "Indoor and outdoor 5G diffraction measurements and models at 10, 20, and 26 GHz," in *2016 IEEE Global Communications Conference (GLOBECOM)*, pp. 1–7, Washington, DC, USA, 2016.

[19] M. Kim, Y. Konishi, Y. Chang, and J. Takada, "Large scale parameters and double-directional characterization of indoor wideband radio multipath channels at 11 GHz," *IEEE Transactions on Antennas and Propagation*, vol. 62, no. 1, pp. 430–441, 2014.

[20] X. Zhou, Z. Zhong, X. Bian et al., "Indoor wideband channel measurements and analysis at 11 and 14 GHz," *IET Microwaves, Antennas & Propagation*, vol. 11, no. 10, pp. 1393–1400, 2017.

[21] C. Ling, X. Yin, H. Wang, and X. Zhang, "Comparison of characteristics of 13–17 GHz propagation channels in indoor environments with different measurement configurations," in *2016 IEEE 27th Annual International Symposium on Personal, Indoor, and Mobile Radio Communications (PIMRC)*, pp. 1–5, Valencia, Spain, 2016.

[22] N. Tran, T. Imai, and Y. Okumura, "Measurement of indoor channel characteristics at 20 GHz band," in *2015 International Symposium on Antennas and Propagation (ISAP)*, pp. 1–4, Hobart, TAS, Australia, 2015.

[23] G. R. Maccartney, T. S. Rappaport, S. Sun, and S. Deng, "Indoor office wideband millimeter-wave propagation measurements and channel models at 28 and 73 GHz for ultra-dense 5G wireless networks," *IEEE Access*, vol. 3, pp. 2388–2424, 2015.

[24] M. Lei, J. Zhang, T. Lei, and D. Du, "28-GHz indoor channel measurements and analysis of propagation characteristics," in *2014 IEEE 25th Annual International Symposium on Personal, Indoor, and Mobile Radio Communication (PIMRC)*, pp. 208–212, Washington, DC, USA, 2014.

[25] S. Geng, J. Kivinen, X. Zhao, and P. Vainikainen, "Millimeter--wave propagation channel characterization for short-range wireless communications," *IEEE Transactions on Vehicular Technology*, vol. 58, no. 1, pp. 3–13, 2009.

[26] A. Hrovat, G. Kandus, and T. Javornik, "Path loss analyses in tunnels and underground corridors," *International Journal of Communication*, vol. 6, no. 3, pp. 136–144, 2012.

[27] "Mobile and wireless communications enablers for the twenty-twenty information society (METIS): METIS channel models," July 2017, https://www.metis2020.com/wp-content/uploads/METIS_D1.4_v3.pdf.

[28] T. S. Rappaport and D. A. Hawbaker, "Wide-band microwave propagation parameters using circular and linear polarized antennas for indoor wireless channels," *IEEE Transactions on Communications*, vol. 40, no. 2, pp. 240–245, 1992.

[29] C. M. P. Ho, T. S. Rappaport, and M. P. Koushik, "Antenna effects on indoor obstructed wireless channels and a deterministic image-based wide-band propagation model for in-building personal communication systems," *International Journal of Wireless Information Networks*, vol. 1, no. 1, pp. 61–76, 1994.

[30] T. S. Rappaport, *Wireless Communications: Principles and Practice*, Prentice-Hall, Upper Saddle River, NJ, USA, 2nd edition, 2002.

[31] A. Hrovat, T. Javornik, and K. Guan, "Analysis of radio wave propagation at millimeter-wave band in tunnels for 5G communications," in *2016 22nd International Conference on Applied Electromagnetics and Communications (ICECOM)*, pp. 1–5, Dubrovnik, Croatia, 2016.